NANOMETER-SCALE ELECTROCHEMICAL PATTERNING OF $LiMn_2O_4$ SURFACES BY AN ATOMIC FORCE MICROSCOPE OPERATING IN AIR

Robert Kostecki[1], Frédéric Bonhomme[2],
Laurent Servant[2], Françoise Argoul[3], Frank McLarnon[1]

[1]Lawrence Berkeley National Laboratory
Berkeley, CA 94720, USA
[2]Laboratoire de Physico-Chimie Moléculaire,
UMR CNRS, Université Bordeaux I,
33405 Talence, France
[3]Centre de Recherche Paul Pascal,
33600 Pessac, France

Abstract

Electrochemical nanometer-scale patterning of the surface of a conducting lithium manganese oxide ($LiMn_2O_4$) by scanning probe microscopy (SPM) was studied. The ability to produce nanometer-size patterns of chemically modified oxide or nanometer-sized alterations of the oxide morphology is demonstrated and discussed with reference to possible mechanisms. It is demonstrated that unlike the SPM-based surface oxidation of metals and semiconductors, the $LiMn_2O_4$ surface is altered *via* electrochemically generated species. We show that a localized surface chemical change can be confined to a depth which depends on the oxide-tip voltage difference and ambient humidity. *In situ* Raman microscopy measurements of localized electrochemical reaction products suggest complex mechanisms of processes induced at the $LiMn_2O_4$ surface, such as delithiation through Li-proton exchange and disproportionation of $LiMn_2O_4$ to MnO_2 and soluble Mn^{2+} species

INTRODUCTION

The idea of generating patterned structures directly on a substrate has many advantages *versus* traditional indirect lithography techniques which involve multiple-step procedures. The ability to position the probe tip with sub-nanometer precision has stimulated efforts to use scanning probe microscopes (SPMs) to fabricate nano-scale features on surfaces [1-6]. SPMs have been used for nanometer-scale lithography on ultra-thin polymer films [7], patterning by local oxidation of hydrogen-passivated silicon surfaces [8,9], fabrication of single-electron transistors by the anodic oxidation of Nb [10], micro-contact printing [11-15], and dip-pen nanolithography [16,17]. However, a significant problem encountered when attempting to fabricate nano-features with conventional atomic force microscopy (AFM) or scanning tunneling microscopy (STM) is the presence of a thin water layer adsorbed or condensed onto the substrate. Such a water layer can interfere with the probe tip motion, however it exhibits very high conductivity [18] and serves as a medium for highly localized electrochemical processes [19,20].

EXPERIMENTAL

We used an AFM to both image and modify the surface of the conducting oxide $LiMn_2O_4$ in air [20]. The AFM tips were coated with thin layers of Pt or W_2C. All AFM experiments were performed in constant-force mode with controlled oxide-tip voltage differences. A single scan of the tip over the oxide surface simultaneously produced two images: a topographic image and a conductance image; the latter represents oxide-tip current variations during scanning at a given oxide-tip voltage difference. Thin (~400 nm) films of $LiMn_2O_4$ were deposited onto Pt or stainless-steel substrates [20]. X-ray diffraction patterns and Raman spectra of the $LiMn_2O_4$ thin films confirmed a cubic spinel structure with a Fd3m space symmetry group and a 0.819 nm cubic cell lattice parameter. Raman microscopy measurements were carried out with a LabRam microscope made by ISA Groupe Horiba.

RESULTS

Figure 1A shows a standard topographic AFM image of a representative 5 x 5 μm area of a $LiMn_2O_4$ surface. A conductance image, represented by the oxide-tip current response of the same area (not shown here) at a -1.0 V voltage difference between the oxide and AFM tip, displayed a uniform current distribution. Throughout this paper we will define a positive oxide-tip voltage difference to mean that the oxide is poised positive relative to the AFM tip, and *vice versa*. The current did not exceed 1.5 nA and its magnitude was determined by the electronic properties of the oxide and the tip, the voltage difference, and the specific geometry of both the tip and the oxide surface.

While experimenting with the AFM and $LiMn_2O_4$ at ambient conditions and at different oxide-tip voltage differences, we observed that the current tended to decrease upon repeated scans over a given area, and it decreased rapidly with time when the tip was immobilized. Importantly, the rate of current decrease at a negative oxide-tip voltage difference was steady and slow, whereas at positive voltage differences the current dropped to zero within a few seconds.

We then selected five separate areas within the same 5 x 5 μm region, and we scanned each of them once at +1.0 V. Figure 1B shows a subsequent AFM image, recorded at -1.0 V, of the same 5 x 5 μm region. The conductance was substantially reduced in the areas scanned at a

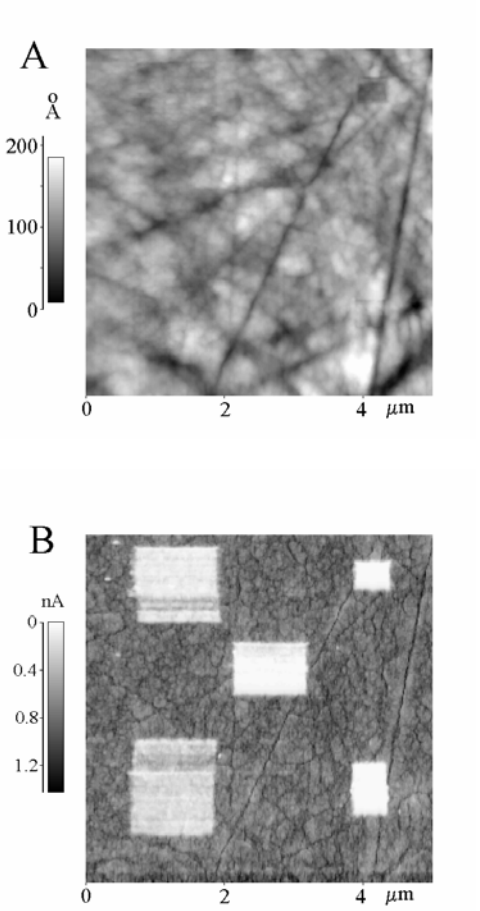

Fig.1. AFM images of surface topography (A) and conductance (B) of a $LiMn_2O_4$ surface (5 X 5 μm) at ambient conditions, recorded at –1.0 V after surface modification of five areas produced at +1.0 V.

positive voltage difference with no visible change in the oxide surface morphology. In contrast to imaging at a negative voltage, a positive voltage caused a rapid decline of film conductance. The fact that the surface conductance declines irreversibly at both positive and negative voltage differences at different rates suggests a similar mechanism, albeit with different process efficiencies. However, by reducing the magnitude of the negative voltage difference to <0.1 V we could suppress the resistance buildup while preserving good contrast of the conductance image. These findings demonstrate that we can use a positive oxide-tip voltage difference to modify the local conductance of the oxide in a controlled manner, *i.e.*, we can "write" with a negatively charged tip, and then "read" the as-produced pattern with a positively charged tip. The as-produced pattern can be erased by scanning over the entire region at positive voltage. We made several successful attempts to modify areas ~20 nm wide, however the relatively high surface roughness made it extremely difficult to generate modified areas of regular geometric shape. The surface conductance modification at ambient conditions was never accompanied by visible (*via* AFM) changes of surface morphology.

Regarding the mechanisms by which AFM modifies the $LiMn_2O_4$ surface electronic properties, the observed asymmetric oxide-to-tip voltage dependence renders abrasion, local heating, and hot-electron-induced reactions rather unlikely but lends strong support to electrochemical processes. The existence of a thin layer of adsorbed water on most materials under ambient conditions has been demonstrated by STM experiments on both conductive and non-conductive samples [18,21-23]. However, there remains a debate on whether the mechanism of charge transfer and image formation in STM experiments under a thin layer of water involves direct electron tunneling or is similar to that in scanning electrochemical microscopy (SECM).

To investigate the role of adsorbed water, a series of experiments in a N_2 atmosphere at controlled relative humidity (RH) levels was carried out. The effect of humidity on the rate of surface modification was dramatic and in direct proportion to the water vapor content. At RH levels close to saturation, the oxide-tip current did not vanish after a scan at positive voltage but remained high during several tens of scans over the same area. Figure 2 presents a set of 5 x 5 μm AFM images (A – topography, B - conductance) recorded at -1.0

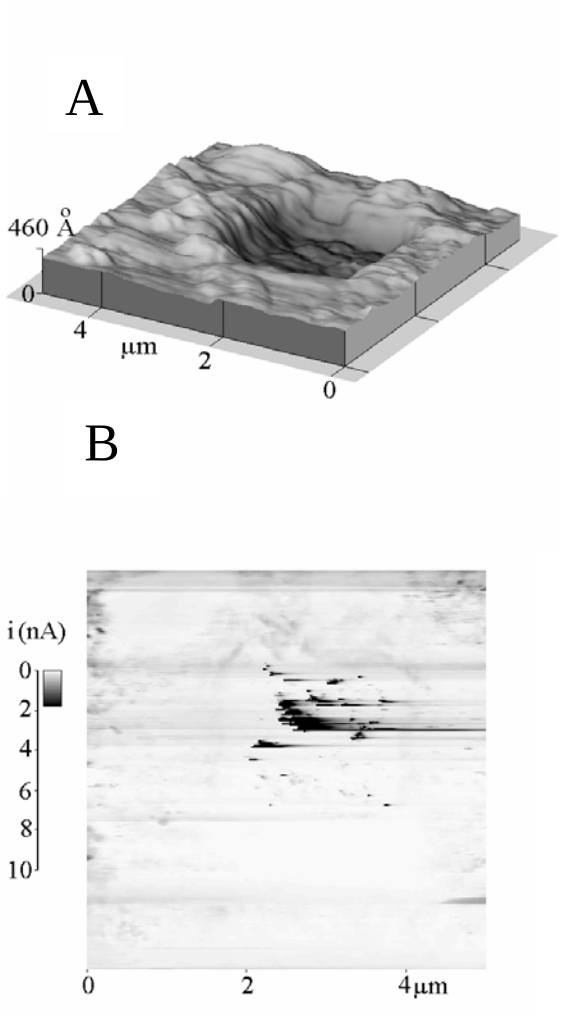

Figure 2. AFM images of surface topography (A) and conductance (B) of a $LiMn_2O_4$ surface recorded at -1.0 V. Surface-localized etching was induced by AFM scanning within a 2x2 μm region (center area of the 5x5 μm image) at +1.0 V in a H_2O-saturated N_2 atmosphere after 40 scans.

V following 40 scans at +1.0 V of a 2 x 2 μm area located in the middle of the 5 x 5 μm region. This experiment was carried out in H_2O-saturated N_2 atmosphere. The topographic image shows that scanning at +1.0 V at high RH led to localized etching of the $LiMn_2O_4$ surface. Prolonged scanning at positive voltage etched a cavity 50 nm deep. The morphology of the region which encircles the 2 x 2 μm area was also modified, mainly due to accumulation of reaction products which were removed from the cavity. The conductance image shows a dramatic increase of the surface resistance not only in the 2 x 2 μm area but also in the surrounding region. The area of very low conductance spread over the entire AFM viewing window, suggesting that the reaction products formed in the hole were dragged away from the cavity by the AFM tip and spilled over the entire region.

The non-conductive character of the reaction products not only renders them detectable by electron-probe methods such as conducting-probe AFM and STM but also limits the reaction penetration depth into the oxide at low-to-moderate ambient RH. The $LiMn_2O_4$ film undergoes a shallow surface transformation at low RH with little or no detectable morphology change. When the water content at the oxide surface is high, *e.g.*, at high RH, the reaction products (which may be either water-soluble or hygroscopic) can be penetrated by the tip and dragged away from the scanned area, thereby exposing fresh $LiMn_2O_4$ material. The observed mounds on the sides of the cavity we created suggest that an electrochemical process combined with abrasive etching created the cavity.

Current-voltage (*i*-V) curves of an immobilized AFM tip in contact with the oxide were reported in [20]. We found that in the absence of water layer (zero relative humidity environment) the current is basically limited only by the resistance of the film. The substantial current increase in the presence of adsorbed water is consistent with a contribution from electrochemical reactions, especially at high voltage. The non-conductive reaction products rapidly formed an electronic barrier between the stationary tip and the oxide.

The writing-reading process and the *i*-V curves exhibited very limited sensitivity to the tip material. In a series of AFM experiments with a W_2C-coated tip very similar and reproducible results were obtained, however the surface modification process proceeded at a slightly higher positive voltage. Because in all cases the tip was in forced contact with $LiMn_2O_4$, an interfacial resistance must cause the oxide-to-tip voltage difference to increase until an electrochemical process could arise at overpotentials specific for the tip and oxide. The resulting electrochemical reactions will be limited to an area determined by the size of the water meniscus between

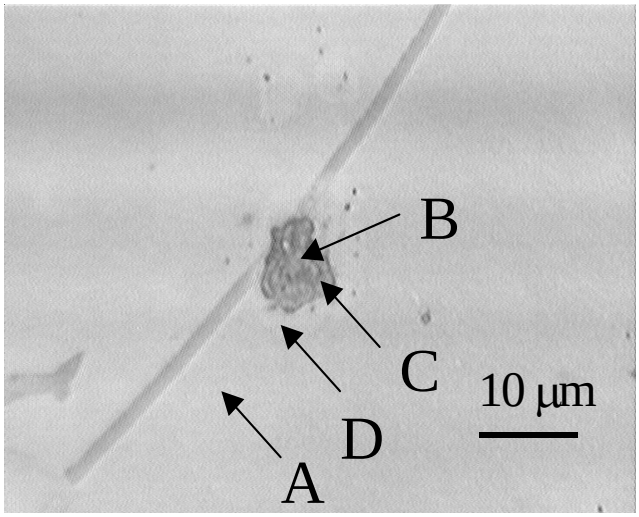

Figure 3. An image of the reaction zone between the Pt tip and the $LiMn_2O_4$ sample. The dark cavity in the image center represents the point of contact. Arrows mark surface sites at which Raman spectra were recorded.

the tip and oxide, as well as the electric field and current distribution in the close vicinity of the tip.

An *in situ* Raman microscopy experiment was carried out to identify local electrochemical reaction products. The AFM tip was replaced with a thin 0.1 mm dia. Pt wire and its sharp end was brought in contact with the $LiMn_2O_4$ electrode. The ambient relative humidity was nearly 100% in this case. A potential difference of 2 V between the $LiMn_2O_4$ sample and the Pt wire was applied, and the electrode surface at the point of contact was observed through the optical microscope and the current response was monitored. The current diminished very quickly from the initial value and vanished completely after 40-50 s of polarization. When the current dropped to zero the Pt wire was removed and Raman microscopy analysis of the modified region was carried out.

Figure 3 shows an optical microscope image of the reaction region which was created in the $LiMn_2O_4$ thin film by the Pt wire at 2 V. The dark area in the image center represents a cavity which was formed at the point of where the Pt wire contacted the sample.

Four Raman spectra were recorded from the reaction zone and its vicinity (Fig. 4). The spectrum of the original material (A) is typical for the $LiMn_2O_4$ spinel and consists of a broad band centered at 630 cm^{-1} and two shoulders at 590 and 655 cm^{-1}. The Raman spectrum taken from the bottom of the cavity (B) shows very similar features however, slight band broadening is observed. Also, a new weak and broad band located at 860 cm^{-1} becomes visible. Dramatic changes in the lithium manganese oxide composition are observed as the Raman probe approaches the edge of the cavity. The spectrum measured at the inner part of the edge (C) shows a strong band at 655 cm^{-1}, which is characteristic for Mn^{3+} oxides and hydroxides. Surprisingly, the spectrum recorded at the outer edge of the cavity (D) in the bright shadow zone which surrounds the cavity displays a sharp peak at 590 cm^{-1} which is characteristic for λ-MnO_2 [24].

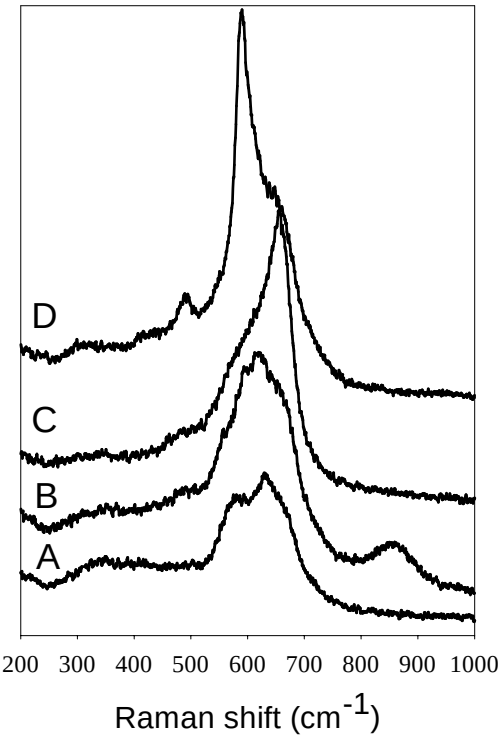

Figure 4. Raman spectra recorded of the reaction zone. Original material (A), bottom of the cavity (B), inner edge of the cavity (C), outer edge of the cavity (D).

It is still difficult to identify the specific electrochemical reactions responsible for modification of the original film at positive (anodic) voltage. Given the products of the $LiMn_2O_4$ conversion, candidate reactions include the direct oxidation of $LiMn_2O_4$ to λ-MnO_2 and Li_2O or LiOH and the simultaneous reduction of water and/or protons at the tip. However, the formation of only λ-MnO_2, which preserves the original cubic spinel

structure of $LiMn_2O_4$, cannot explain the observed film dissolution and production of at least partially soluble manganese compounds at high RH. Another conceivable mechanism involves water oxidation at the $LiMn_2O_4$ film, which can lead to a local decrease of pH and subsequent disproportionation of $LiMn_2O_4$ into Mn(II) and λ-MnO_2 [24]. Thus, the original $LiMn_2O_4$ structure will break down, and Mn(II) and Li ions will contribute to the solution meniscus ion conductivity and/or precipitate in the form of salts and/or hydroxides to form a non-conductive electronic barrier. The thickness and structure of the water layer (which depend on RH) determine the extent and rate of this process.

In summary, we demonstrated the use of contact AFM for nanometer-scale electrochemical lithography of thin $LiMn_2O_4$ films. Although we used only $LiMn_2O_4$ films in this study, this novel approach may be used to develop electrochemical reaction schemes to image and modify other inorganic and organic materials which may be used for the direct fabrication and detection of nanometer-scale patterns.

ACKNOWLEDGMENT

This work was supported by the Director, Office of Energy Research, Office of Basic Energy Sciences, Chemical Sciences Division of the U.S. Department of Energy under Contract No. DE-AC03-76SF00098 and the Berkeley-France Fund.

REFERENCES

1. G.M. Shedd and P.E. Russel, *Nanotechnology*, **1**, 67 (1990)
2. "Electrochemical Nanotechnology", edited by W.J. Lorenz and W. Plieth, Wiley-VCH, 1998.
3. D.M. Eigler and E.K. Schweizer, *Nature*, **344**, 524 (1990)
4. I-W. Lyo, Ph. Avouris, *Science*, **253**, 173 (1991)
5. H.J. Mamin, P.H. Guethner and D. Rugar, *Phys. Rev. Lett*., **65**, 2418 (1990).
6. Y. Utsugi, *Nature*, **347**, 747 (1990)
7. M.A. McCord, R.F. Pease, *J.Vac.Sci Technol*. **B6**, 293 (1988)
8. J. A. Dagata, J. Schneir, H. H. Harary, C. J. Evans, M. T. Postek and J. Bennet, *Appl. Phys. Lett*., **56**, 2001 (1990)
9. N. Barniol, F. Perez-Murano, X. Aymerich, *Appl. Phys. Lett*., **61**, 462 (1992)
10. J-I. Shirakashi, K. Matsumoto, N. Miura, M. Konagai, *Appl. Phys. Lett*., **72**, 1893 (1998)
11. A. Majumdar, P.I. Oden, L.A. Nagahara, J. J. Graham and J. Alexander, *Appl. Phys. Lett*., **61**, 2293 (1992)
12. L. Tsau, D. Wang, and K. L. Wang, *Appl. Phys. Lett*., **64**, 2133 (1994)
13. A. Kumar, H.A. Biebuyck, N. L. Abbot, G. M. Whitesides, *J. Am. Chem. Soc.* **114**, 9188 (1992)
14. R.J. Jackman, J.L.Wilbur, G.M. Whitesides, *Science* **269**, 664 (1995)
15. Y. Xia, J.A. Rogers, K.E. Paul, G.M. Whitesides, *Chem. Rev.* **99**, 1823 (1999)
16. R. D. Piner, J. Zhu, F. Xu, S. Hong, C.A. Mirkin, *Science*, **283**, 661 (1999)
17. S. Hong, J. Zhu, C.A. Mirkin, *Science*, **286**, 523 (1999)
18. R. Gluckenberger, M. Heim, G. Cevc, H. F. Knapp, W. Wiegräbe, A. Hillebrand, *Science*, **266**, 1538 (1994)

19. A. J. Bard, F.-R. F. Fan and M. V. Mirkin, *Electroanalytical Chemistry*, A. J. Bard Ed. (Dekker, New York, 1994), vol. 18, pp. 243-373
20. R. Kostecki, F. McLarnon, *Appl. Phys. Lett*., **76**, 2536 (2000)
21. M. Heim, R. Eschrlich, A. Hillebrand, H. F. Knapp, R.Gluckenberger, *J. Vac. Sci. Technol. B*, **14**, 1498 (1996)
22. M. Luna, F.Rietord, N. A. Melman, Q. Dai, M. Salmeron, *J. Phys. Chem. A*, **102**, 6793 (1998)
23. F. F. Fan, A. J. Bard, *Science*, **270**, 1849 (1995)
24. J. C. Hunter, *J. Solid State Chem.*, **39**, 142 (1981)